A Complete Fully Thin-Film PV Harvesting and Power-Management System on Plastic With On-Sheet Battery Management and Wireless Power Delivery to Off-sheet Loads

Warren Rieutort-Louis, *Student Member, IEEE*, Liechao Huang, *Student Member, IEEE*,
Yingzhe Hu, *Student Member, IEEE*, Josue Sanz-Robinson, Sigurd Wagner, *Fellow, IEEE*,
James C. Sturm, *Fellow, IEEE*, and Naveen Verma, *Member, IEEE*

***Abstract*—Large-area electronics enables the creation of systems with transformational capabilities and form factors. Through the ability to integrate thin-film photovoltaics, batteries, and active transistors, complete power-management subsystems addressing a wide range of applications can also be created. We present, for the first time, a fully flexible system integrating amorphous silicon (a-Si) solar modules with Li-ion thin-film batteries and circuits that are based on a-Si thin-film transistors for battery management and wireless power delivery. A fabricated prototype of the entire system on a plastic sheet is demonstrated. Using a 240 cm^2 solar module under indoor lighting conditions ($\sim$400 μW/cm^2), the system is measured to provide 1) dc power ($\sim$1 mW) to on-sheet loads and 2) ac power ($\sim$10 mW) to off-sheet loads through wireless transmission. Four Li-ion batteries are used for on-sheet energy storage with a battery-management system ensuring discharging at permissible levels, while imposing minimal off-state current ($<$360 nA).**

***Index Terms*—Amorphous semiconductors, battery management systems, energy-harvesting, flexible electronics, photovoltaic systems, thin-film circuits, thin-film transistors.**

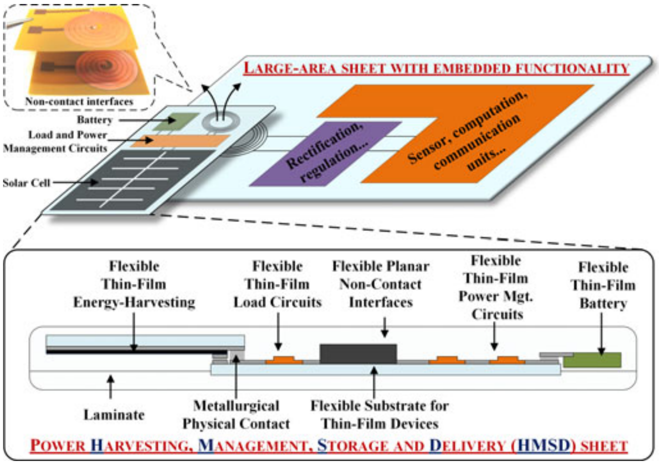

Fig. 1. System concept and physical assembly of power harvesting, management, storage, and delivery (HMSD) sheet system components making use of sheet lamination.

I. INTRODUCTION

THROUGH the deposition of thin-film devices at low temperatures, large-area electronics (LAE) enables the creation of transformational systems with novel form factors on flexible sheets. The simultaneous ability to form amorphous silicon (a-Si) energy-harvesting devices [e.g., photovoltaics (PV)], thin-film transistors (TFTs), thin-film diodes (TFDs), and passives (e.g., inductors, capacitors, resistors) can enable complete self-powered systems for a wide range of embedded applications. Flexible sheets that are based on PV harvesters with integrated a-Si TFT power electronics for wireless charging of personal devices are such an application, for which two systems have recently been reported. The first system [1] uses two solar modules (dc) from which current is switched in turn by TFTs in order to generate an oscillating output (ac) for transfer over a noncontact capacitive link, while the second system [2] uses a TFT-based *LC* oscillator to transfer power over a noncontact inductive link.

However, to exploit the highly promising sensing and actuation capabilities within LAE [3] in complete systems, integrated thin-film subsystems for continuous power-management are required, by combining energy harvesting with local energy storage (i.e., to account for periods of diminished illumination of, e.g., solar modules). In this study, we present a fully thin-film sheet that accomplishes this.

Fig. 1 illustrates the system concept, showing the proposed power harvesting, management, storage, and delivery (HMSD) sheet for wireless power delivery to large-scale systems (e.g., a large-area sheet with embedded functionality). Interfacing to general large-area sheets is simply achieved by placing the HMSD sheet onto a power-receiving surface without the need for complex metallurgical connections. The aim is a generalized

---

Manuscript received June 10, 2013; revised August 3, 2013; accepted September 26, 2013. Date of publication October 30, 2013; date of current version December 16, 2013. The work of W. Rieutort-Louis was supported by the IBM Ph.D. Fellowship and the Princeton Andlinger Center Maeder Graduate Fellowship in Energy and the Environment. This work was supported by the National Science Foundation under Grant ECCS-1202168 and Grant CCF-1218206.

The authors are with the Department of Electrical Engineering and the Princeton Institute for the Science and Technology of Materials, Princeton University, Princeton, NJ 08544 USA (e-mail: rieutort@princeton.edu; liechaoh@princeton.edu; yingzheh@princeton.edu; jsanz@princeton.edu; wagner@princeton.edu; sturm@princeton.edu; nverma@princeton.edu).

Color versions of one or more of the figures in this paper are available online at http://ieeexplore.ieee.org.

Digital Object Identifier 10.1109/JPHOTOV.2013.2285959

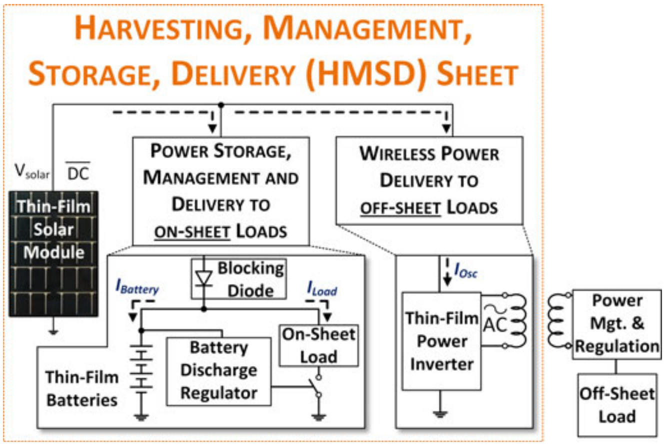

Fig. 2. Schematic representation of the HMSD harvesting, management, storage, and delivery sheet system architecture.

and easy-to-integrate platform for powering various large-area sheets; a flexible HMSD sheet ensures that power delivery is not constrained by the physical form factor of the large-area sheet. In addition to PV harvesters and power inverters for wireless power delivery, the HMSD sheet comprises a TFT-based subsystem for management of commercial, flexible, thin-film lithium-ion batteries, thus also enabling local energy storage and continuous powering of on-sheet loads.

The inset in Fig. 1 shows the physical assembly of the various components of the HMSD sheet. The use of lamination provides a path for low-cost integration of batteries and multiple free-standing substrates onto which on-sheet a-Si thin-film components (e.g., PV, TFTs, TFDs) are patterned. Conductive adhesive [e.g., anisotropic conductive film (ACF)] provides low-resistance, mechanically robust contact between the illustrated planes.

In this paper, we describe all the components of the HMSD sheet, with particular focus on circuits and devices to meet two key requirements of the sheet. First is the need for reliable and safe charging of the thin-film batteries from dc-output solar modules as well as the protection of these batteries from excessive discharge during on-sheet load powering. Second is the need for off-sheet power delivery from solar cells; for this, the dc power output is converted to ac via a thin-film power inverter whose power-transfer efficiency is enhanced by operating beyond the TFT f_t frequency limit [2].

II. SYSTEM ARCHITECTURE

Fig. 2 shows a block diagram of the HMSD sheet. The solar module consists of a-Si solar cells in series operating at an output voltage V_{solar}. DC power from the module is distributed on the large-area sheet to

1) an *on-sheet* power-storage, management, and delivery block that comprises batteries, a battery-discharge-regulator subsystem, and on-sheet loads;
2) an *off-sheet* power-delivery block that comprises an inverter for wireless power delivery to off-sheet loads (with their own local energy-storage/regulation circuits).

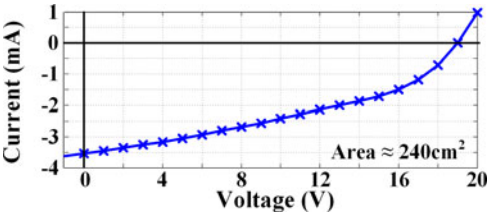

Fig. 3. Solar module *I–V* characteristic under interior illumination.

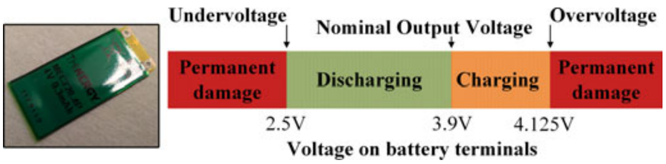

Fig. 4. Permissible operating voltages for charging and discharging of thin-film Li-Ion batteries.

Under solar illumination, dc current is supplied to both the on-sheet and off-sheet power blocks. In the former, the supplied current is split between charging the batteries (I_{Battery}) and delivering power to the on-sheet load (I_{Load}), while in the latter, current is delivered to the oscillator (I_{Osc}). Without illumination, current is supplied from the batteries to the on-sheet load and the off-sheet block is not operational.

Section III describes the key components and devices that are required for the HSMD sheet. Sections IV and V describe the detailed operation of the on-sheet and off-sheet power-management blocks, respectively.

III. KEY COMPONENTS REQUIRED FOR THE HARVESTING, MANAGEMENT, STORAGE, AND DELIVERY SHEET

A. Flexible Thin-Film Solar Modules

Commercial a-Si solar modules fabricated on a 50-μm-thick polymer substrate are used for system demonstration purposes. A typical measured *I–V* characteristic under indoor lighting conditions ($\sim$400 μW/cm^2) is shown in Fig. 3. The thin-film circuitry on the HMSD sheet typically draws modest current levels and, as such, the operating point is close to the open-circuit voltage of the solar module V_{solar} of 19 V.

B. Flexible Thin-Film Batteries

Commercial flexible thin-film lithium-ion (Li-ion) batteries [4] are used for energy storage. These are based on a lithium cobalt oxide cathode, a lithium metal anode, and a lithium phosphorus oxynitride electrolyte. As is typical with Li-ion battery technology, achieving safe and reliable charging/discharging is conditional on drawing charge from (or supplying charge to) the battery within a well-defined window of operating voltages. Failure to do so would result in permanent battery damage. Fig. 4 illustrates the permissible operating voltage range for the thin-film batteries used inthe HMSD system, with an open-circuit (nominal output) voltage of 3.9 V.

A method of managing the power drawn from the batteries is thus required to ensure that once the battery reaches the

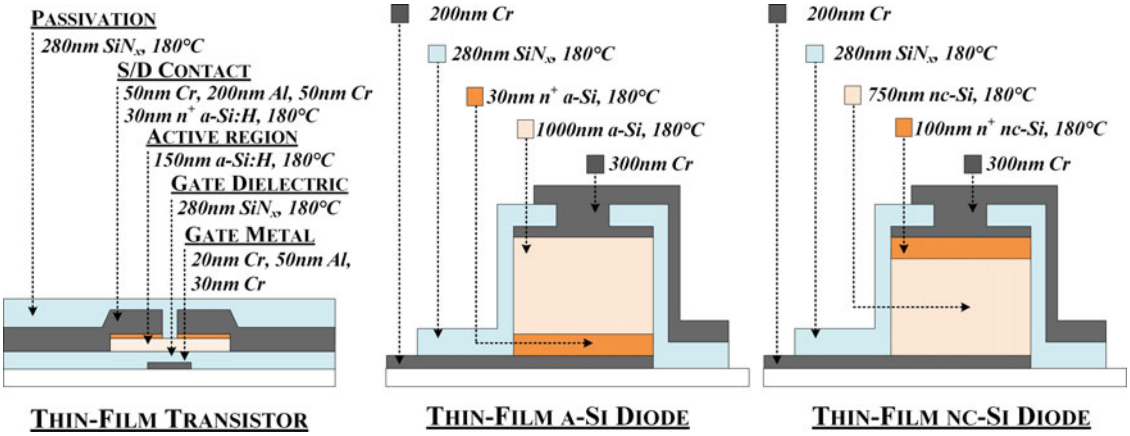

Fig. 5. a-Si TFT and a-Si/nc-Si TFD device structures.

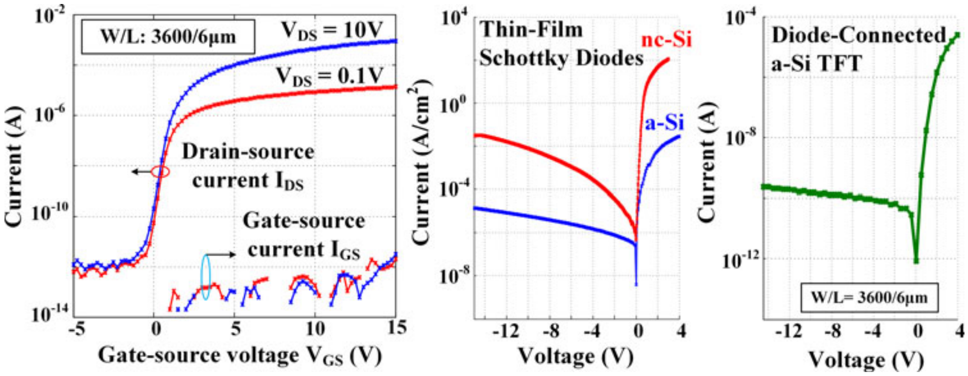

Fig. 6. Thin-film transistor and thin-film diode characteristics.

under-voltage condition, any load is cut off, preventing further battery discharge until the battery has been partly or fully recharged.

C. Flexible, Thin-Film Circuit Technology

A wide variety of materials and processes exist that enable the fabrication of circuits directly patterned on flexible substrates such as polymers or metallic foils. These include, for example, amorphous silicon, organics [5], or metal oxides [6]. For the HMSD sheet, a-Si is used as the primary semiconducting material; its proven commercial viability and established industrial processing on sheets up to 10 m^2 make it an attractive candidate for a wide range of emerging flexible-system applications.

Our four-chamber PECVD a-Si manufacturing capability allows for the processing of 7.5 cm × 7.5 cm square, 50-μm-thick polyimide substrates onto which the following devices are patterned: thin-film transistors (TFTs), thin-film diodes (TFDs—using amorphous or nano-crystalline Si), thin-film diode-connected transistors, and thin-film resistors (TFRs). Circuits constructed from these components were shielded from light to minimize off-state leakage. Typical device structures and characteristics are shown in Figs. 5 and 6, respectively.

Back-channel etched TFTs are optimized for processing on plastic, with typical channel length of 6 μm; large thin-film resistors (for low static current in the battery-management circuit) are made using n$^+$ a-Si with sheet resistance of 30 MΩ/sq [7], [8]. Thin-film a-Si and nc-Si Schottky TFDs [9] are optimized for large on–off ratio as shown; Schottky diodes are used instead of p-i-n diodes due to their simpler fabrication, avoiding the use of p-type thin-film silicon which is not part of a standard a-Si process as used in production of TFT AMLCD technologies. These diodes, where used, are fabricated separately and mounted onto the flexible sheet. From the perspective of power-management circuits, a number of considerations arise due to the performance limitations of the thin-film devices [7]. Table I summarizes the design challenges for circuits.

TABLE I
CHALLENGES FOR a-Si TFT POWER CIRCUITS

PROPERTY	CAUSE	IMPLICATION
Low transconductance ($g_m \sim 9\times10^{-5}$ A/V for W/L=600, $V_{ds}=V_{gs}=10$V)	Disordered a-Si structure, low electron mobility (~1 cm^2/Vs), high threshold voltages ($V_T \sim 2.5$V)	Low-current switches
Only NMOS TFTs	Low field-effect hole mobility (<0.1 cm^2/Vs)	CMOS topologies not viable
Large device parasitic capacitances	Large device features and process margins for processing on free-standing substrates	Reduced performance and increased switching losses

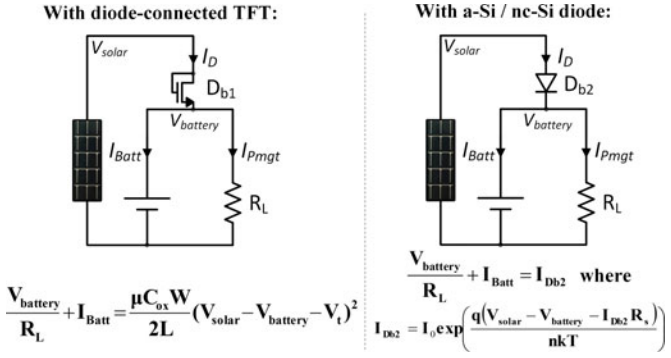

Fig. 7. Options for the blocking diode interfacing the battery management circuitry with the solar module using either diode connected thin-film transistors or thin-film diodes.

IV. POWER REGULATION AND DELIVERY TO ON-SHEET LOADS

In this section, the subsystems of the HMSD sheet for power storage, power management, and power delivery to on-sheet-loads will be discussed.

A. Interfacing With the Solar Module: Blocking Diode Design

The blocking diode (D_b) prevents leakage from the batteries under low-illumination conditions (i.e., when $V_{\rm solar}$ drops). It could be implemented using either diode-connected TFTs (attractive from an integration perspective), or either a-Si or nc-Si Schottky diodes, as shown in a generalization of the power-management block circuit in Fig. 5. A first evaluation of the performance of the blocking diode can be made by studying the circuit behavior under a range of different loads R_L. For small resistive loads, $V_{\rm battery}$ droops due to the voltage drop across the blocking diode required to sustain $I_{\rm Pmgt}$.

A critical condition can be identified where, for a given solar module voltage $(V_{\rm solar})$, $V_{\rm battery}$ has drooped to the point that the charging current $(I_{\rm Batt})$ drops to zero (at which point $V_{\rm battery}$ is simply the nominal output voltage of the stack of batteries). This point sets the minimum resistive load that can be powered by the on-sheet block and, thus, serves as a performance metric for the system. When using a diode connected TFT (which is connected to always be in saturation when above V_t), this occurs when:

$$R_L < \frac{V_{\rm battery\,(nominal)}}{\frac{\mu C_{ox} W}{2L}(V_{\rm solar} - V_{\rm battery\,(nominal)} - V_t)^2} \qquad (1)$$

whereas for the case of an a-Si or nc-Si diode, this occurs when

$$R_L < \frac{V_{\rm battery\,(nominal)}}{I_{Db2}} \qquad (2)$$

where I_{Db2} is defined in Fig. 7, including the diode series resistance component *Rs*.

A second evaluation of the performance is necessary however, considering the reverse leakage current of the blocking diode under the low-illumination condition. Here, nearly the full nominal voltage of the batteries appears across D_{b1}/D_{b2}; an excessive reverse leakage can result in permanent damage of the batteries due to draining as described previously. An analysis of the three diode options is provided in Section VI.

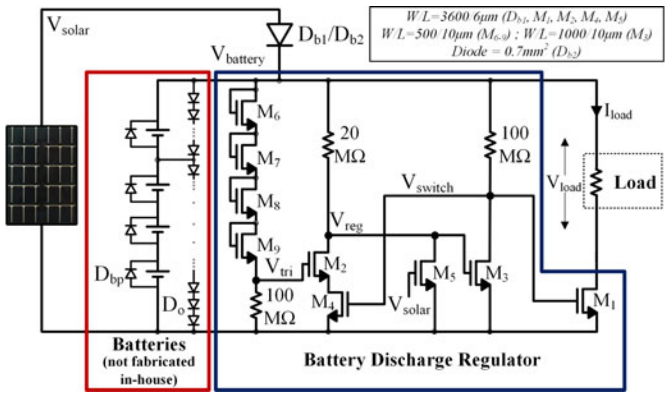

Fig. 8. HMSD sheet subblocks for power storage, management, and delivery to on-sheet loads.

B. Thin-Film Battery Discharge Regulator

Fig. 8 shows the details of the battery-discharge regulator block. This block is connected to the solar module through the charge-blocking diode, D_{b1}, and it gates the current provided to an on-sheet load through the use of M_1 to ensure safe discharge levels for the batteries. For analysis, a purely resistive load is used to represent on-sheet loads; in practice, these could be embedded functionality circuits (e.g., sensing, power metering. . .)

Four series-connected 300 μAh thin-film Li-ion batteries as previously described are used for energy storage, providing a nominal output voltage $V_{\rm battery}$ of 15.6 V. This value is chosen to satisfy the voltage-level requirements in typical thin-film circuits. The diode stack D_o ensures proper charging conditions for the batteries, while the TFT circuit $(M1–M9)$ is used to ensure proper discharging conditions during load powering. During charging, the batteries may not be exposed to a charging voltage greater than ~16.5 V (4 × 4.125 V); to ensure this, a chain of current-shunting diodes D_o provides regulation if this voltage is exceeded. Bypass diodes D_{bp} are typically included in parallel with each battery to ensure current continuity if one battery fails.

Under low illumination, the batteries take over powering of the load. During discharging, the nominal output voltage of the batteries is maintained until the batteries approach their fully discharged state. At this point, the output voltage begins to drop rapidly; however, following from previous discussion, a drop below ~10 V (4 × 2.5 V) must be prevented to avoid permanent battery damage.

A low-voltage cut-off circuit is thus implemented, as shown in Fig. 8, to provide rapid turn-off of the load current via a regenerative circuit. $V_{\rm tri}$ follows the battery voltage through the voltage drop across a chain of diode-connected TFTs M_{6-9}. During battery powering, M_2 and M_4 are initially “ON,” pulling $V_{\rm reg}$ low; however, the M_{6-9} chain is designed such that when the battery voltage drops below 10 V, $V_{\rm reg}$ rises, thereby pulling $V_{\rm switch}$ low through M_3. This causes M_4 to begin to turn OFF,

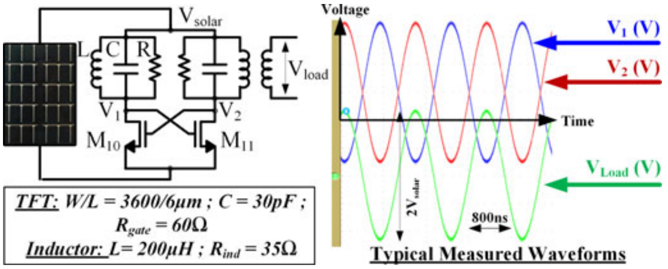

Fig. 9. Circuit diagram, typical device parameters, and measured waveforms of the *LC*-oscillator inverter for wireless off-sheet power delivery using planar inductors.

triggering regeneration on $V_{\rm reg}$ and $V_{\rm switch}$. This causes the load current to turn OFF through rapid control of the power TFT M_1.

With full-swing regeneration on $V_{\rm switch}$, a large on-to-off ratio of 10^5 for the battery current can thus be achieved through M_1 control. Activation of M_1 is subsequently achieved by resetting the circuit through M_5. With M_5 controlled by $V_{\rm solar}$, battery discharge is prevented until after the battery has been partly/fully recharged, following the return of illumination.

In the "OFF" state, current results primarily from static current through the branches of the regenerative stages and through M_1. M_1's current can be handled as described in the following section, while the current through the regenerative stages can be minimized through sizing of the associated thin-film resistors. After low-voltage cut off occurs, the normal battery operating voltage is redeveloped on $V_{\rm battery}$ and maintained due to the lower current being drawn, with an effective small increase in battery capacity [4]. The width of M_1 is designed so that the level of leakage current is such that low-voltage battery failure would not occur until after *at least* 100 h. For an application, this can be set as desired to be much longer than the expected interval expected between daily illumination periods.

C. Power-Delivery to On-Sheet Load

To design the power-TFT M_1, two optimal conditions can be considered. First, the optimal power point for the load is achieved when M_1 imposes a voltage drop equivalent to the load voltage, i.e., $V_{M1} = V_{\rm load} = V_{\rm battery}/2$. Second, the optimal power delivery efficiency is achieved when M_1 exhibits minimal voltage drop. However, this requires either reduction of the load current (and, therefore, load power) or reduction of the effective TFT resistance through increased M_1 width or through an array of parallel-connected TFTs. Though viable, this could increase the off-state leakage and can thus only be pursued to levels permitted by battery discharge limits and expected illumination-cycle periods.

V. Wireless Power Delivery to Off-Sheet Loads

Fig. 9 shows the details of the block for wireless power-delivery to off-sheet loads. This block consists of an *LC* oscillator-based on-sheet inverter [2], enabling inductive coupling for wireless power delivery to an off-sheet load.

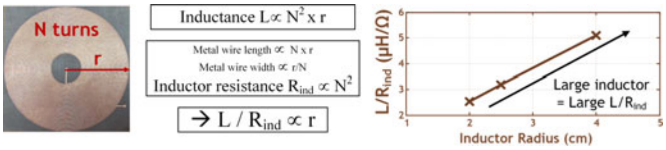

Fig. 10. Design and optimization of the L/$\rm R_{ind}$ ratio of copper planar inductors leveraging large-area inductor sizes to achieve *LC* oscillator operation and wireless power transfer.

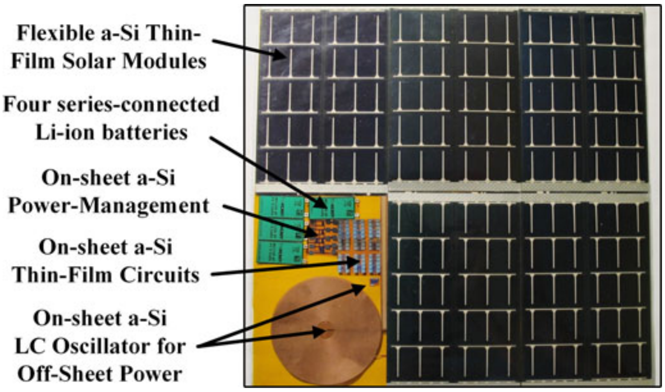

Fig. 11. System prototype on a flexible polyimide sheet (20 × 15 cm) showing the assembled thin-film components: solar modules, batteries, thin-film circuits, and wireless power transfer inductors.

The *LC* oscillator allows operation above the f_t of the TFTs by resonating out the large device parasitic capacitances C. The ability to pattern physically large inductors leads to high-quality factors, thus enabling the resonant tank to be achieved efficiently (i.e., with large effective tank resistance).

In order for oscillations to occur, a positive feedback condition must be satisfied [2].

$$\frac{g_m}{C} \times \frac{L}{R_{\rm ind} + R_{\rm gate}} > 1. \tag{3}$$

While this condition depends in part on the modest TFT electrical properties described earlier (low g_m, high gate-source/drain capacitances contributing to C, and large TFT bottom-gate resistance $R_{\rm gate}$) which can be optimized only to a limited extent [7], the ability to pattern large (cm-scale) inductor coils enables high inductance and small resistance as shown in Fig. 10. This enables robust oscillations, despite the limitations of the TFT devices and their parasitics.

Methods for increasing the output power [2] include increasing solar-module voltage or optimizing TFT-width for the specific loads expected on the large-area sheet that is receiving the power.

VI. Experimental Results

The entire PV-based HMSD sheet is fabricated on 50 μm-thick polyimide, at a maximum temperature of 180 °C. The system prototype is shown in Fig. 11, while the thin-film-circuit micrograph is in Fig. 12, and a system performance summary is in Table II.

Experimental results for all the subsystems are now presented

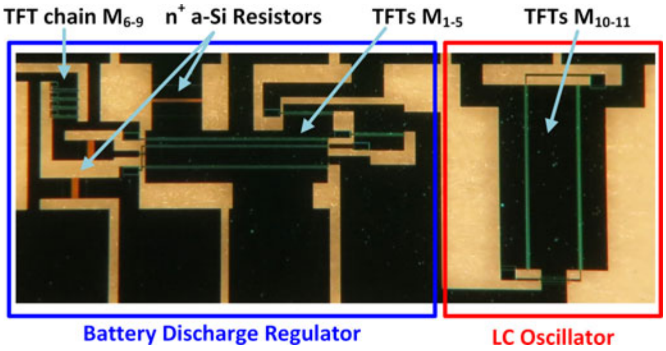

Fig. 12. Micrographs of HMSD thin-film circuits (10 × 5 mm).

TABLE II
HMSD Sheet System Performance Summary

a-Si Solar Module	V_{oc}=19V, Area=240cm^2, Under indoor illumination=0.4mW/cm^2
Batteries	4 x Li/LiCoO$_2$/LiPON, 300µAh, 3.9V 2.5V<Operating voltage per battery<4.12V
On-Sheet load power	~1.2 mW to 150kΩ
Largest on-sheet load	150kΩ with a 0.7mm^2 a-Si blocking diode
On-sheet standby current	240nA (circuit) + 120nA (blocking diode)
Off-Sheet max. load power	~10mW to 10kΩ at 21% transfer efficiency
Off-Sheet transmission	Frequency ≈ 2MHz, 2cm-radius inductors

TABLE III
Performance Metrics for Blocking Diode Options

Blocking Diode	***Metric 1:*** **On-Current Delivery to Load**	***Metric 2:*** **Rev. Leakage at -15.6V**
Diode connected TFT (W/L = 3600/6 µm)	For V_{gs}=V_{ds}=3.4V, I_d=10µA → **Minimum R_L=1.5MΩ**	< 500pA
a-Si Schottky Diode (Area = 1 mm^2)	For V_d=3.4V, I_d=200µA → **Minimum R_L=80kΩ**	~ 100nA
nc-Si Schottky Diode (Area = 0.01 mm^2)	For V_d=2V, I_d=5mA → **Minimum R_L=3kΩ**	~3 µA

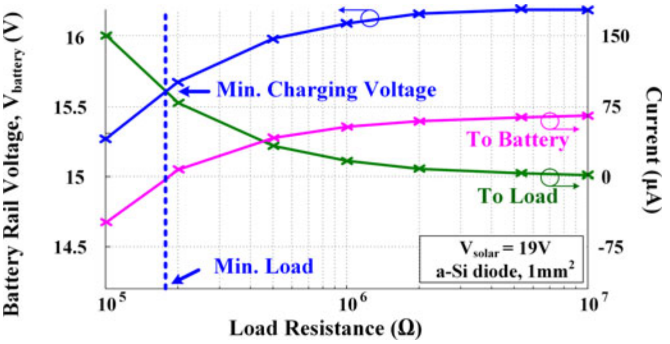

Fig. 13. Measured effect of blocking diode voltage drop on battery-charging current.

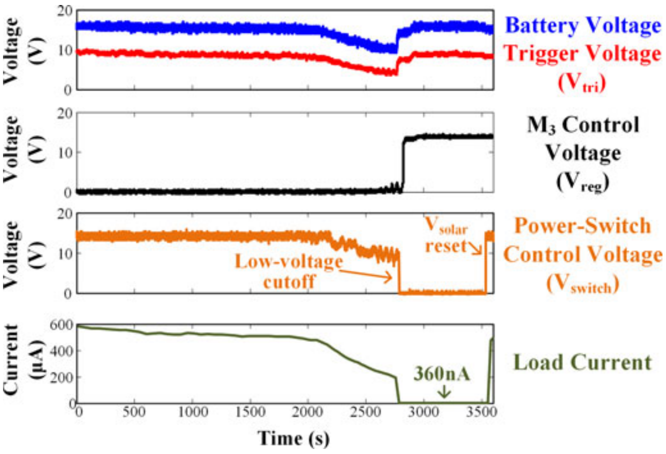

Fig. 14. Measured waveforms for on-sheet power delivery.

A. Power Regulation and Delivery to on-Sheet Loads

1) Thin-Film Blocking Diode Optimization: A comparison of the three blocking diode options is performed in Table III using the performance metrics described in Section IV, with $V_{\text{battery}} = 15.6$ V and $V_{\text{solar}} = 19$ V for the TFT-based and a-Si Schottky diodes (leading to a 3.4 V allowable diode-voltage drop). For the nc-Si diodes, a $V_{\text{solar}} = 17.5$ V is used for comparison as voltage drops larger than 3 V are unreliably sustained due to the large current densities achieved.

While the diode-connected TFT provides an attractive on-current to reverse-leakage ratio, for practical TFT dimensions, the on-current is lower than the manufactured a-Si diodes. The a-Si Schottky diode used in this system provides good forward current ($\sim$200 μA) when the solar module is charging the battery and powering the load, while giving a reverse leakage ($\sim$100 nA at -15.6 V), which is reasonable, in that it is of the same order as the static leakage through the power-management block, as will be described later. The diode size could be increased further to support higher load currents at the cost of proportionally higher reverse leakage. The nc-Si diode has a better on–off ratio, potentially allowing for slightly better forward current; however, depending on the required reverse leakage conditions, very small diodes ($<$0.0005 mm^2) might be required, which are challenging to manufacture.

Fig. 13 shows the drop on the battery-voltage rail that arises due to voltage drops across the blocking diode D_{b1} (a-Si, 1 mm^2 diode) as the load current increases (i.e., due to reduced on-sheet loads).

With a 0.7 mm^2 a-Si TFD, loads less than 150 kΩ are still powered, but the voltage on V_{battery} falls below 15.6 V and is no longer sufficient to provide charging current to the batteries.

2) Thin-Film Battery Discharge Regulator: Fig. 14 shows measured waveforms for the on-sheet battery discharge regulator subsystem. For testing, power at a level of $\sim$5 mW is delivered for 45 min from the batteries to a 10 kΩ load.

As the battery is discharged, the nominal output voltage is initially maintained, but beyond 40 min, it begins to decrease. Once V_{battery} reaches the critical-discharge level ($\sim$10 V), the low-voltage cutoff circuit triggers, and the load current is disabled by the power TFT M_1. Subsequently, the current drawn from the batteries drops to below 360 nA, protecting the battery from further discharge.

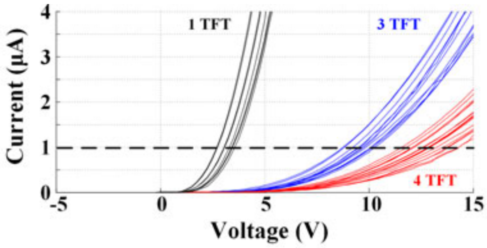

No. of Diode-Connected TFTs	1	3	4
Voltage drop: Mean	3.2 V	9.6 V	12.9 V
Voltage drop: St. Dev.	0.3 V	0.5 V	0.8 V

Fig. 15. TFT diode chain variability statistics at $I_{\text{diode-chain}} = 1\ \mu$A.

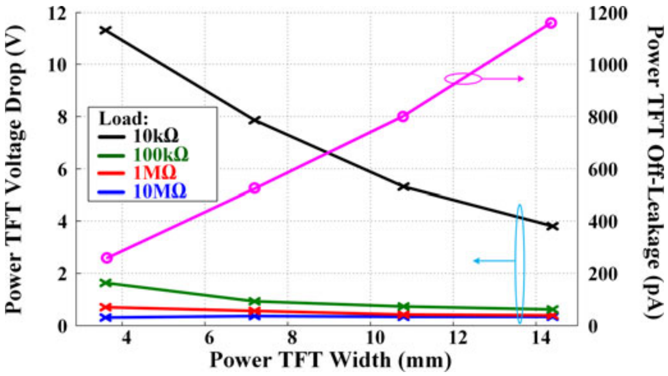

Fig. 16. Tradeoffs of power-TFT M_1 voltage drop and off-leakage incurred through scaling of the M_1 TFT width.

At this point, the voltage of the batteries returns to a level close to the nominal output voltage due to the greatly reduced current being drawn. A reset through M_5 arising from renewed solar-module illumination is also shown.

The variability of the M_{6-9} voltage drop (i.e., due to TFT threshold-voltage variation) could potentially shift the trigger point; however, measurements across many diode chains found that the range required to ensure correct regeneration can reliably be achieved with modest margining, as set by the standard deviations shown in Fig. 15.

3) Thin-Film Battery Discharge Regulator: Fig. 16 shows how the voltage drop across the power TFT switch scales with the width of the switch (implemented as parallel TFTs for testing performed without charge-blocking diode D_{b1}).

Wider switches result in reduced drops and large V_{load}; however, as shown, this comes at the cost of larger off-state leakage current (shown for $V_{\text{drop}} = 15.6$ V). In the prototyped design, however, this leakage is very small compared with the leakage due to the regenerative branches of the cut-off circuit.

As discussed in Section IV, two optimization approaches may be considered for power delivered to the on-sheet load, optimal power delivery, or power delivery efficiency.

Fig. 17 illustrates this tradeoff whereby with larger resistive loads higher delivery efficiency is achieved at the expense of power delivered to the load.

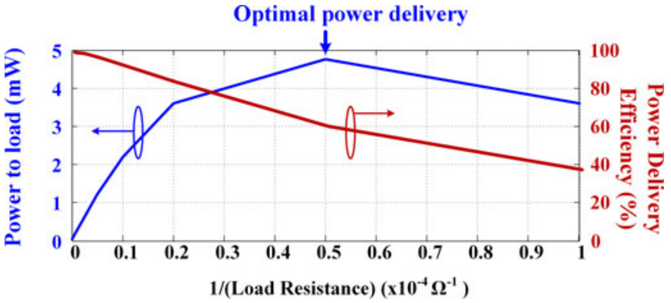

Fig. 17. Tradeoff of power delivered versus power delivery efficiency to on-sheet loads.

B. Wireless Power Delivery to Off-Sheet Loads

The *LC* oscillator delivers power wirelessly (at 2 MHz) to an off-sheet resistive load via 2 cm-radius patterned 25-μm-thick copper inductors. The inductors could be monolithically fabricated onto the HMSD sheet through an additive process but, for this system demonstration, are fabricated separately and mounted for testing. At a V_{solar} of 19 V and at 1 mm separation distance from the load, the *LC* oscillator delivers 8 mW (under indoor lighting conditions) with 21% power-transfer efficiency, drawing power directly from the solar module.

VII. CONCLUSION

A fully thin-film power harvesting, management, storage, and delivery (HMSD) sheet is demonstrated based on PV harvesters. It delivers power both locally to an on-sheet battery, battery-management system, and load, as well as wirelessly to off-sheet loads through an *LC*-oscillator-based power inverter. The use of thin-film batteries enables the continuous operation of embedded systems under temporary conditions of reduced illumination. For reliable battery operation, integrated circuitry for controlling the charging and discharging conditions on the batteries is demonstrated, enabling milliwatt-level output power with low off-state leakage.

REFERENCES

[1] L. Huang, W. Rieutort-Louis, Y. Hu, J. Sanz-Robinson, S. Wagner, J. Sturm, and N. Verma, “Integrated all-silicon thin-film power electronics on flexible sheets for ubiquitous wireless charging stations based on solar-energy harvesting,” in *Proc. VLSI Symp. Circuits*, Honolulu, HI, USA, Jun. 13–15, 2012, pp. 198–199.

[2] Y. Hu, W. Rieutort-Louis, L. Huang, J. Sanz-Robinson, S. Wagner, J. Sturm, and N. Verma, “Flexible solar-energy harvesting system on plastic with thin-film LC oscillators operating above ft for inductively-coupled power delivery,” in *Proc. Custom Integrated Circuits Conf.*, San Jose, CA, USA, Sep. 2012.

[3] T. Someya, B. Pal, J. Huang, and H. E. Katz, “Organic semiconductor devices with enhanced field and environmental responses for novel applications,” *MRS Bulletin*, vol. 33, pp. 690–696, 2008.

[4] *THINERGY MEC220*, Infinite Power Solutions, Littleton, CO, USA, Dec. 7–9, 2009.

[5] T. Someya, T. Sekitani, M. Takamiya, T. Sakurai, U. Zschieschang, and H. Klauk, “Printed organic transistors: Toward ambient electronics,” in *Proc. Int. Electron. Device Meeting*, Baltimore, MD, USA, Dec. 7–9, 2009, pp. 1–6.

[6] D. A. Zhao, D. A. Mourey, and T. N. Jackson, “Flexible plastic substrate ZnO thin film transistor circuits,” in *Proc. Device Res. Conf.*, Jun. 22–24, 2009, pp. 177–178.

[7] W. Rieutort-Louis, J. Sanz-Robinson, Y. Hu, L. Huang, J. C. Sturm, N. Verma, and S. Wagner, "Device optimization for integration of thin-film power electronics with thin-film energy-harvesting devices to create power-delivery systems on plastic sheets," presented at the Int. Electron Device Meeting, San Francisco, CA, USA, Dec. 2012, Paper 12.3.

[8] B. Hekmatshoar, K. H. Cherenack, A. Z. Kattamis, K. Long, S. Wagner, and J.C. Sturm, "Highly stable amorphous-silicon thin-film transistors on clear plastic," *Appl. Phys. Lett.*, vol. 93, no. 3, Jul. 2008.

[9] J. Sanz-Robinson, W. Rieutort-Louis, N. Verma, S. Wagner, and J. Sturm, "Frequency dependence of amorphous silicon schottky diodes for large-area rectification applications," in *Proc. 70th Device Res. Conf.*, Jun. 18–20, 2012, pp. 117–118.

Warren Rieutort-Louis (S'12) received the B.A. (Hons.) and M.Eng. degrees in electrical and information engineering from Trinity College, Cambridge University, Cambridge, U.K. in 2009 and the M.A. degree in electrical engineering from Princeton University, Princeton, NJ, USA, in 2012, where he is currently working toward the Ph.D. degree.

His research interests include thin-film materials, processes, devices and circuits for large-area electronic systems, as well as the development of hybrid thin-film/complementary metal–oxide semiconductor systems.

Mr. Rieutort-Louis received an IBM Ph.D. Fellowship and the Andlinger Center Maeder Fellowship in Energy and the Environment. He is a Graduate Teaching Fellow with the Princeton McGraw Center for Teaching and Learning.

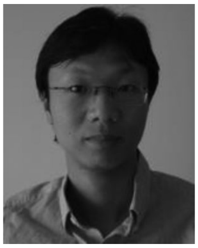

Liechao Huang (S'12) received the B.S. degree in microelectronics from Fudan University, Shanghai, China, in 2010 and the M.A. degree in electrical engineering from Princeton University, NJ, USA, in 2012, where he is currently working toward the Ph.D. degree.

His research interests include thin-film circuit design for power, radio and sensing interfaces, complementary metal–oxide semiconductor (CMOS) analog and mixed signal design for sensing interfaces and power management and hybrid system design combining thin-film circuits and CMOS integrated circuits.

Mr. Huang received a 2010-2011 Princeton Fellowship.

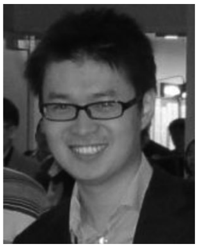

Yingzhe Hu (S'12) received the B.S. degrees in both physics and microelectronics from Peking University, Beijing, China, in 2009 and the M.A. degree in electrical engineering from Princeton University, Princeton, NJ, USA, in 2011, where he is currently working toward the Ph.D. degree.

His research interests include thin-film circuit and integrated circuit hybrid sensing system design and analog and mixed signal design for sensing interfaces.

Mr. Hu received a 2013 Qualcomm Innovation Fellowship.

Josue Sanz-Robinson received the B.Eng. degree in electrical engineering (Hons.) from McGill University, Montreal, QC, Canada, in 2010 and the M.A. degree in electrical engineering from Princeton University, Princeton, NJ, USA, in 2012, where he is currently working toward the Ph.D. degree in electrical engineering.

His research interests include amorphous/nanocrystalline silicon rectifying diodes and sensors for flexible large-area electronic systems.

Mr. Sanz-Robinson received a 2013 Qualcomm Innovation Fellowship.

Sigurd Wagner (SM'78–F'00) received the Ph.D. degree from the University of Vienna, Vienna, Austria, in 1968.

He was a Postdoctoral Fellow with Ohio State University, Columbus, OH, USA. From 1970 to 1978, he was with the Bell Telephone Laboratories, working on semiconductor memories and heterojunction solar cells, and from 1978 to 1980, he was the Chief of the Photovoltaic Research Branch of the Solar Energy Research Institute (now NREL), Golden, CO, USA. Since 1980, he has been a Professor of electrical engineering, Princeton University, Princeton, NJ, USA, developing materials, processes, and components for flexible large-area electronics, electrotextiles, and electronic skin. He is currently working on backplanes using amorphous and nanocrystalline silicon on plastic and steel foil substrates, elastomeric interconnects and circuit boards, flexible permeation barriers and gate dielectrics, and functional cells for flexible electronics.

Dr. Wagner is a Fellow of the American Physical Society. He received the Nevill Mott Prize "for his groundbreaking research, both fundamental and applied, on amorphous semiconductors as well as chalcopyrites" in 2009.

James C. Sturm (S'81–M'85–SM'95–F'01) received the B.S.E. degree in electrical engineering and engineering physics from Princeton University, Princeton, NJ, USA, and the M.S.E.E and Ph.D. degrees in electrical engineering from Stanford University, Stanford, CA, USA, in 1981 and 1985, respectively.

He was with Intel Corporation as Microprocessor Design Engineer, as well as with Siemens, Munich, Germany. He has been with the Faculty of Princeton University since 1986, where he is currently a Professor of electrical engineering and PRISM Director. During 1994–1995, he was a von Humboldt Fellow with the Institüt Für Halbleitertechnik, University of Stuttgart, Stuttgart, Germany. He has worked in the fields of silicon-based heterojunctions, 3-D integration, silicon-on-insulator, optical interconnects, TFT's, and organic light-emitting diodes. His current research interests include silicon–germanium–carbon and related heterojunctions on silicon, SOI, and 3-D integration, large-area electronics, flat-panel displays, organic semiconductors, and the nanotechnology–biology interface.

Dr. Sturm is a member of the American Physical Society and the Materials Research Society. Formerly, he was a National Science Foundation Presidential Young Investigator. He received ten awards for teaching excellence from both Princeton University and the Keck Foundation and received the President's Distinguished Teaching Award at Princeton in 2004. In 1996 and 1997, he was the Technical Program Chair and General Chair of the IEEE Device Research Conference, for which he is now a charter trustee. He served on the organizing committee of IEDM (1988–1992 and 1997–1999), having chaired both the Solid-State Device and Detectors/Sensors/Displays committees. In 2005, he was named the William and Edna Macaleer Professor of Engineering and Applied Science. He also has been a symposium organizer for the Materials Research Society and on the SOS/SOI, EMC, and several other conference committees. He was the organizing Chair for ISTDM 2006.

Naveen Verma (S'03–M'09) received the B.A.Sc. degree in electrical and computer engineering from the University of British Columbia, Vancouver, BC, Canada, in 2003 and the M.S. and Ph.D. degrees in electrical engineering from the Massachusetts Institute of Technology, Cambridge, MA, USA, in 2005 and 2009, respectively.

Since July 2009, he has been an Assistant Professor of electrical engineering with Princeton University, Princeton, NJ, USA. His research interests include advanced sensing systems, including low-voltage digital logic and SRAMs, low-noise analog instrumentation and data-conversion, large-area sensing arrays based on flexible electronics, and low-energy algorithms for embedded inference, especially for medical applications.

Dr. Verma received/co-received the 2006 DAC/ISSCC Student Design Contest Award, the 2008 ISSCC Jack Kilby Paper Award, the 2012 Princeton Innovation Forum First Prize, the 2012 Alfred Rheinstein Princeton Junior Faculty Award, the 2013 NSF CAREER Award, and the 2013 Intel Early Career Award.